

Emergent electronic and magnetic state in $\text{Ca}_3\text{Ru}_2\text{O}_7$ induced by Ti doping

X. Ke,^{1,*} J. Peng,² D. J. Singh,³ Tao Hong,¹ Wei Tian,⁴ C. R. Dela Cruz,¹ and Z. Q. Mao²

¹Neutron Scattering Science Division, Oak Ridge National Laboratory, Building 8600, MS6473, Oak Ridge, Tennessee 37831, USA

²Department of Physics and Engineering Physics, Tulane University, New Orleans, Louisiana 70118, USA

³Materials Science and Technology Division, Oak Ridge National Laboratory, Oak Ridge, Tennessee 37831, USA

⁴Ames Laboratory and Department of Physics and Astronomy, Iowa State University, Ames, Iowa 50011, USA

(Received 3 October 2011; published 4 November 2011)

We report an emergent electronic and magnetic state in the bilayer ruthenate $\text{Ca}_3\text{Ru}_2\text{O}_7$ upon doping with a small concentration of Ti on the Ru sites. In contrast to a quasi-two-dimensional metallic state in $\text{Ca}_3\text{Ru}_2\text{O}_7$, which has an antiferromagnetic (AF) state formed by ferromagnetic (F) bilayers stacked antiferromagnetically along the c -axis, we find an insulating ground state with a “G”-type nearest-neighbor AF order in $\text{Ca}_3(\text{Ru}_{1-x}\text{Ti}_x)_2\text{O}_7$ for $x \geq 0.03$. The close proximity of these two distinct electronic and magnetic states demonstrates unique competing magnetic interactions in $\text{Ca}_3\text{Ru}_2\text{O}_7$, which provides a rare opportunity to investigate the interplay between correlated metal physics and Mott physics.

DOI: 10.1103/PhysRevB.84.201102

PACS number(s): 71.27.+a, 71.15.Mb, 71.30.+h, 75.25.-j

Competition between different magnetic tendencies in metals is thought to play a key role in emergent phenomena, including unconventional superconductivity. Examples include the Fe-based superconductors, where competing magnetic tendencies are thought to lead to a weakened spin-density wave state that gives way to high temperature superconductivity^{1,2} and the single-layer ruthenate Sr_2RuO_4 , which has competing ferromagnetic (F) and antiferromagnetic (AF) tendencies³ that give way to an unconventional superconducting state, most likely a triplet state.⁴

Sr_2RuO_4 and the related ruthenates, $(\text{Sr}_{1-x}\text{Ca}_x)_{n+1}\text{Ru}_n\text{O}_{3n+1}$, provide an excellent opportunity for unraveling the physics of such competitions. These materials exhibit various remarkable states such as triplet superconductivity (Sr_2RuO_4),⁵ a novel nematic electronic state ($\text{Sr}_3\text{Ru}_2\text{O}_7$),⁶ and a Fermi surface-driven metal-insulator transition (MIT) in $\text{Ca}_3\text{Ru}_2\text{O}_7$.⁷ In addition to these states that are associated with the metallic physics, ruthenates also involve physics of localized states associated with the orbitals, including superexchange and tendencies towards orbital ordering, as manifested by the orbital-ordered Mott-insulating antiferromagnet, Ca_2RuO_4 .^{4,8} These rich properties of ruthenates reflect the essential role of competing magnetic interactions. Two types of magnetic competitions have been identified in ruthenates: (1) competition between states associated with distinct Fermi-surface instabilities, such as the competition between F and incommensurate AF fluctuations in Sr_2RuO_4 ³ and $\text{Sr}_3\text{Ru}_2\text{O}_7$;⁹ (2) competition between the antiferromagnetism due to Mott transition and the itinerant ferromagnetism due to Stoner instability in $\text{Ca}_{2-x}\text{Sr}_x\text{RuO}_4$.⁸ The competition of various ground states in ruthenates also manifests itself in the sensitivity of their ground states to external stimuli, such as chemical doping, pressure, etc.

Ti doping into Ru sites has been used as an important means in investigating the nature of competing magnetic interactions in ruthenates. Ti^{4+} is nonmagnetic and has similar ionic radius as Ru^{4+} such that Ti doping should introduce little lattice distortion but nonetheless strongly scatters charge carriers at the Fermi level and is thus disruptive to the magnetic interactions. In both Sr_2RuO_4 and $\text{Sr}_3\text{Ru}_2\text{O}_7$ a small amount of Ti doping yields unexpected incommensurate spin-density

wave ordering,^{10,11} indicating that these two materials are near a quantum critical point associated with the interplay of F and AF fluctuations.¹²

$\text{Ca}_3\text{Ru}_2\text{O}_7$ is known to possess very rich physics as well. It undergoes a paramagnetic-AF transition around $T_N \sim 56$ K, followed by a MIT at $T_{\text{MIT}} \sim 48$ K.¹³ Interestingly it is found the conductivity of $\text{Ca}_3\text{Ru}_2\text{O}_7$ shows a metallic behavior along the in-plane directions below T_{MIT} , indicating the existence of a non-negligible number of itinerant charge carriers.¹⁴ This is indeed demonstrated by the ARPES experiments,⁷ which reveal a small Fermi-surface pocket surviving at low temperatures and by the optical conductivity measurements as well.¹⁵ This is associated with the particular magnetic structure^{16–18} of $\text{Ca}_3\text{Ru}_2\text{O}_7$ consisting of F bilayers that couple antiferromagnetically to each other, the latter of which results in spin-valve type conductivity. Pressure-effect studies on $\text{Ca}_3\text{Ru}_2\text{O}_7$ show that a high pressure applied within the ab -plane weakens the MIT accompanied with the occurrence of a possible new magnetic phase transition.¹⁹ Moreover, recent angle-resolved magnetoresistance measurements reveal that the change of magnetic field orientation can induce complex magnetic phase transitions.²⁰ These results imply that $\text{Ca}_3\text{Ru}_2\text{O}_7$ may involve competing magnetic interactions.

Here, we report an emergent magnetic ground state induced by a small amount of Ti doping in $\text{Ca}_3\text{Ru}_2\text{O}_7$. While the magnetic structure of $\text{Ca}_3(\text{Ru}_{0.97}\text{Ti}_{0.03})_2\text{O}_7$ appears to be the same as the one for the pure compound at $T_{\text{MIT}} < T < T_N$, $\text{Ca}_3(\text{Ru}_{0.97}\text{Ti}_{0.03})_2\text{O}_7$ shows a G-type AF spin structure within the bilayer below T_{MIT} accompanied with an insulating transport behavior along both in-plane and c axes. This is in sharp contrast to the spin structure featured by F bilayers coupled antiferromagnetically along the c -axis in the pristine compound. This G-type AF state is accompanied by a dramatic magnetoelastic coupling effect. These findings, in conjunction with density functional calculations, suggest that $\text{Ca}_3\text{Ru}_2\text{O}_7$, which shows competition between different states associated with Fermi-surface instabilities, is also on the borderline of a very distinct non-Fermi surface-driven magnetic instability, making it a fascinating system for studying the interplay of correlated metal physics and Mott physics.

Single-phase $\text{Ca}_3(\text{Ru}_{0.97}\text{Ti}_{0.03})_2\text{O}_7$ single crystals were grown using a floating-zone technique. The Ti-doping concentration of the samples was verified using the Energy Dispersive Spectroscopy method. Magnetization and transport measurements were conducted using a superconducting quantum interference device (SQUID) magnetometer and a physical property measurement system (PPMS), respectively. Neutron diffraction experiments were performed using HB1A thermal neutron triple-axis spectrometers at High Flux Isotope Reactor (HFIR) at Oak Ridge National Laboratory. The neutron incident energy E_i was fixed as 14.64 meV, and data were taken with collimations of 48'-48'-sample-40'-68'. A high-quality single-domain single crystal sample with a mass of ~ 0.15 gram was cooled down using a closed-cycle He fridge. Orthorhombic crystal structure indices of the material were used, and the sample was measured in the $(H\ 0\ L)$ and $(0\ K\ L)$ scattering planes, where $H, K,$ and L are the reciprocal lattice indices. Nuclear Bragg diffraction requires H (K) and L be even or the sum of H and L be even.

Figure 1(a) shows the temperature dependence of magnetic susceptibility for $\text{Ca}_3(\text{Ru}_{0.97}\text{Ti}_{0.03})_2\text{O}_7$. It clearly shows two transitions occurring at $T_N \sim 62$ K and $T_{\text{MIT}} \sim 45$ K, corresponding to the paramagnetic-AF transition and the MIT, respectively, as in the pure $\text{Ca}_3\text{Ru}_2\text{O}_7$.^{13,14} The Curie-Weiss temperatures derived from fits over $240\text{ K} < T < 300\text{ K}$ are -46 K, -123 K, and -68 K along $a, b,$ and c -axes,

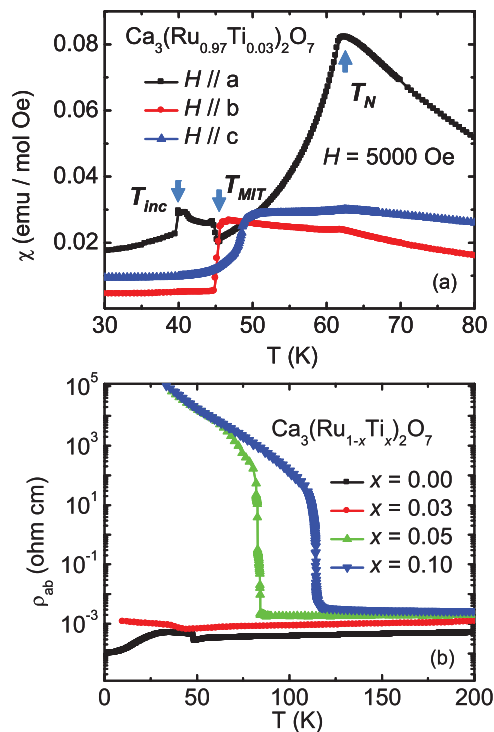


FIG. 1. (Color online) (a) Temperature dependence of magnetic susceptibility of $\text{Ca}_3(\text{Ru}_{0.97}\text{Ti}_{0.03})_2\text{O}_7$ measured with 5000 Oe field. The data were measured while warming up after an initial zero-field cool. Arrows denote the onset of magnetic transitions. (b) In-plane resistivity ρ_{ab} as a function of temperature for $\text{Ca}_3(\text{Ru}_{1-x}\text{Ti}_x)_2\text{O}_7$ with different x values. The transport data were measured using a standard four-probe technique with a dc current $I = 1$ mA applied along the $[110]$ direction.

respectively. This is distinct from the positive Curie-Weiss temperature reported in $\text{Ca}_3\text{Ru}_2\text{O}_7$, which exhibits F in-plane coupling.²¹ Figure 1(b) shows the in-plane resistivity ρ_{ab} as a function of temperature for $\text{Ca}_3(\text{Ru}_{1-x}\text{Ti}_x)_2\text{O}_7$ with different x values. It is seen that $\text{Ca}_3(\text{Ru}_{0.97}\text{Ti}_{0.03})_2\text{O}_7$ displays an insulating conductivity behavior below T_{MIT} , which is in contrast to the in-plane metallic feature¹⁴ observed in the undoped sample. Hysteresis in the transport measurements (Fig. S2 in the supplementary materials) indicates the first-order character of the MIT. The MIT feature becomes much more remarkable with increasing x . The in-plane resistivity of the 5% and 10% Ti-doped samples, which have the same low-temperature magnetic structure as the 3% Ti-doped sample (see subsequent discussion), increases by ~ 8 orders of magnitude below T_{MIT} . This result, together with the observation of zero-electronic specific heat,²² indicates that the insulating behavior observed in the Ti-doped sample results from an electronic gap opening. Future spectroscopy measurements, such as angular resolved photoemission spectroscopy and optical conductivity, are desirable to directly probe the electronic gap value. Furthermore, a third magnetic transition is observed in $\text{Ca}_3(\text{Ru}_{0.97}\text{Ti}_{0.03})_2\text{O}_7$ at $T \sim 40$ K, as clearly evidenced by the abrupt change in the magnetic susceptibility [Fig. 1(a)] with the magnetic field applied along the a -axis, which is not observed in $\text{Ca}_3\text{Ru}_2\text{O}_7$.

Several magnetic diffraction peaks of $\text{Ca}_3(\text{Ru}_{0.97}\text{Ti}_{0.03})_2\text{O}_7$ were measured. The integrated intensity as a function of temperature is shown in Fig. 2(a). As mentioned previously, $(0\ 0\ 5)$, $(1\ 0\ 2)$, and $(0\ 1\ 3)$ do not satisfy the nuclear Bragg diffraction condition. Also plotted is the $(0\ 0\ 5)$ magnetic Bragg peak of the pure $\text{Ca}_3\text{Ru}_2\text{O}_7$, which reflects its magnetic structure with $(0\ 0\ 1)$ propagation wave vector.^{16,17} Compared to the monotonic increase in the magnetic scattering density

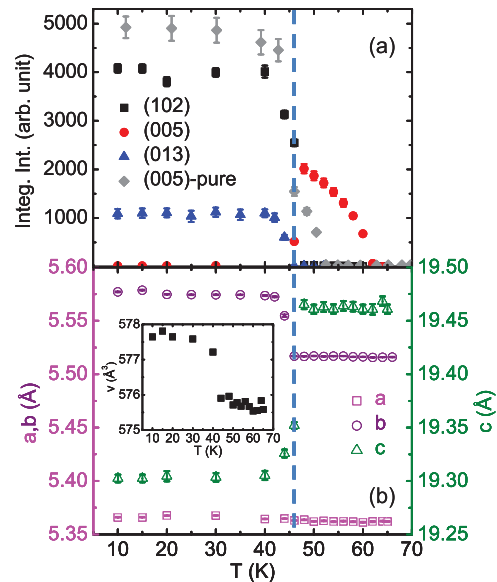


FIG. 2. (Color online) (a) Temperature dependence of the integrated intensity of the magnetic Bragg reflections measured via neutron diffractions: $(1\ 0\ 2)$, $(0\ 0\ 5)$, and $(0\ 1\ 3)$ of $\text{Ca}_3(\text{Ru}_{0.97}\text{Ti}_{0.03})_2\text{O}_7$. Diamond symbols in grey represent the data for $\text{Ca}_3\text{Ru}_2\text{O}_7$. (b) Lattice constant as a function of temperature. Inset shows the temperature dependence of the unit cell volume of $\text{Ca}_3(\text{Ru}_{0.97}\text{Ti}_{0.03})_2\text{O}_7$. The dashed line marks the MIT.

of (0 0 5) in $\text{Ca}_3\text{Ru}_2\text{O}_7$ due to the localization of electrons below T_{MIT} , intriguingly, the (0 0 5) magnetic scattering intensity of $\text{Ca}_3(\text{Ru}_{0.97}\text{Ti}_{0.03})_2\text{O}_7$ has a sharp drop to near zero, while two new magnetic Bragg diffractions along (0 1 3) and (1 0 2) emerge below T_{MIT} . This suggests the occurrence of a new magnetic structure in $\text{Ca}_3(\text{Ru}_{0.97}\text{Ti}_{0.03})_2\text{O}_7$ at low temperatures, which is different from that of pure $\text{Ca}_3\text{Ru}_2\text{O}_7$.

We measured a series of magnetic diffraction peaks both below and above T_{MIT} , in order to resolve the magnetic structure of $\text{Ca}_3(\text{Ru}_{0.97}\text{Ti}_{0.03})_2\text{O}_7$ in different temperature regimes. We found that at $T_{\text{MIT}} < T < T_N$, the spin structure of $\text{Ca}_3(\text{Ru}_{0.97}\text{Ti}_{0.03})_2\text{O}_7$ is the same as that of pure $\text{Ca}_3\text{Ru}_2\text{O}_7$, i.e., spins within the bilayer are ferromagnetically aligned with AF order between the bilayers,^{16,17} as shown in Fig. 3(a). Intriguingly, we find²³ that $\text{Ca}_3(\text{Ru}_{0.97}\text{Ti}_{0.03})_2\text{O}_7$ exhibits a G-type nearest-neighbor AF structure [Fig. 3(c)] below T_{MIT} compared to the F-aligned bilayers for pure $\text{Ca}_3\text{Ru}_2\text{O}_7$ shown in Fig. 3(b); the obtained saturated magnetic moment is about $1.65(0.2) \mu_B/\text{Ru}$, close to the theoretical value for the ($S = 1$) low-spin state of Ru^{4+} ions, with the moment direction tilted approximately 70° from both the a - and c -axes. A similar G-type AF ground state is observed in the 5% and 10% Ti-doped samples. The MIT stated previously is apparently associated with the AF ordering of spins within the layer planes and has a different nature compared to the insulating state in pure $\text{Ca}_3\text{Ru}_2\text{O}_7$, which still has low energy charge excitations.

Figure 2(b) shows the temperature dependence of lattice parameters of $\text{Ca}_3(\text{Ru}_{0.97}\text{Ti}_{0.03})_2\text{O}_7$. While there is no noticeable change in the lattice parameters directly below T_N , both b and c change significantly with an opposite sign below T_{MIT} , and a only increases slightly. Although a similar trend is also observed in $\text{Ca}_3\text{Ru}_2\text{O}_7$, the changes in both b and c in the Ti-doped sample are about $+1.1\%$ and -0.85% , respectively, much larger than that reported in $\text{Ca}_3\text{Ru}_2\text{O}_7$ ($\sim \pm 0.1\%$).¹⁶ The chemical unit cell volume shows a larger negative thermal expansion as well, as shown in the inset of Fig. 2(b). This implies that the RuO_6 octahedra is dramatically compressed, as confirmed by neutron powder-diffraction measurements on a $\text{Ca}_3(\text{Ru}_{0.95}\text{Ti}_{0.05})_2\text{O}_7$ powder sample. That is, the apical Ru-O bond length decreases while the in-plane Ru-O bond length increases, accompanied with a decrease in the Ru-O-Ru

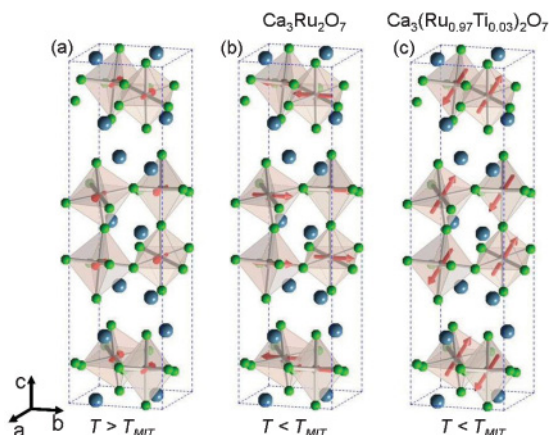


FIG. 3. (Color online) Schematics of the magnetic structure (a) above T_{MIT} , (b) below T_{MIT} for $\text{Ca}_3\text{Ru}_2\text{O}_7$, and (c) below T_{MIT} for $\text{Ca}_3(\text{Ru}_{0.97}\text{Ti}_{0.03})_2\text{O}_7$.

bond angle within the intrabilayer, indicating that octahedral tilting enhances below T_{MIT} . Such remarkable RuO_6 octahedral flattening and tilting are expected to lift the degeneracy of the t_{2g} orbitals and lead to a possible orbital-ordered state, as seen in Ca_2RuO_4 .^{8,24}

We performed density functional theory (DFT) calculations with the generalized gradient approximation of Perdew, Burke, and Ernzerhoff²⁵ and using the rietveld refinement results for the crystal structure of the Ti-doped materials.²³ The calculations were done using the general potential linearized augmented planewave (LAPW) method²⁶ with the augmented planewave plus local orbital modification,²⁷ as implemented in the WIEN2k code.²⁸ The core electrons were treated relativistically, while a scalar relativistic treatment was used for the valence states. We employed a four formula-unit supercell based on a doubling of the primitive cell to the conventional cell.

Calculations were performed both with Ru only and with one Ru replaced by Ti. For the pure Ru case we find energetics and ordering of the magnetic states similar to that obtained previously,¹⁸ even though the structure is now distorted to that of the Ti-doped AF phase. In particular the lowest energy state is that with half-metallic F bilayers stacked antiferromagnetically, which is close in energy to the fully F state. Also similar to the structure of the pure compound, the strongest F interactions are those between the layers comprising the bilayer. The calculated energies with the refined structure relative to the fully F state on a per formula unit basis are -4 meV (ground state), $+133$ meV (C, nearest neighbor AF layers, F intrabilayer ordering), $+89$ meV (A, F layers, AF intrabilayer stacking), and $+163$ meV (G, nearest neighbor AF). The densities of states at the Fermi energy, $N(E_F)$, on a per formula unit basis are 4.2 eV^{-1} , 4.2 eV^{-1} , 9.6 eV^{-1} , 5.7 eV^{-1} , and 9.4 eV^{-1} for the ground state and F, C, A, and G, respectively. This reflects the metallic Stoner mechanism, which is enhanced by double exchange,¹⁸ yielding a reduced $N(E_F)$ for the F orderings relative to the AF orderings. In particular, the G-type ordering is disfavored by the electrons at the Fermi energy and furthermore there is no tendency towards gap opening at the DFT level even when the structure of the AF insulating phase is used. Therefore we may conclude (1) the transition to the G-type structure is not Fermi-surface driven, and (2) the material is far from this state at the bare DFT level, meaning that beyond DFT correlations, most likely Mott physics is responsible.

Calculations with one Ru replaced by Ti show the effect of Ti at the band-structure level. Independent of magnetic order, the Ti occurs as Ti^{4+} with the Ti d bands above the Fermi energy, similar to what was found in Sr_2RuO_4 ,¹² where a Mott state is induced by Ti alloying, although $\sim 20\%$ replacement of Ru is required in that material.²⁹ We find that there is very little contribution of Ti to $N(E_F)$, independent of the magnetic order of the neighboring Ru. The resulting disruption of the hopping in the Ru-O network at a Ti site (note that on the Ti sites there are no d orbitals near E_F to hop through) narrows the bands and modifies the moments on the neighboring atoms (Fig. 4). However, even at the high Ti concentrations in our DFT calculations, the calculated DFT ground state consisting of F bilayers is in disagreement with experiment and again pointing to the essential role of Mott physics in the observed transition. Therefore we conclude that the main effect of

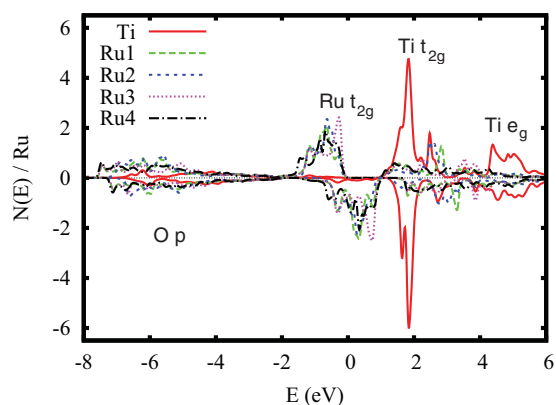


FIG. 4. (Color online) Projections of the d contributions to the density of states for different atoms in a ferromagnetic supercell with one Ru replaced by Ti. The projections are onto the LAPW spheres of radius 2.05 bohr, and the energy zero is at E_F . Ru1, Ru2, and Ru3 are in the same bilayer as the Ti, while Ru4 is in the other bilayer in the supercell, which is practically the same as in the pristine compound. Ru1 is connected to the Ti through the apical O, Ru2 is in the same layer as the Ti, and Ru3 is the remaining Ru in the non-Ti-containing layer. Note the narrow Ti t_{2g} contribution to the DOS well above the Fermi energy and the narrowing of the DOS projections on Ru1, Ru2, and Ru3 relative to Ru4.

Ti substitution is to disrupt hopping, narrow the bands, and lead to a Mott transition. The remarkable fact is that a very low Ti concentration is needed to induce this transition, and furthermore this transition also takes place as a function of temperature with modest T_{MIT} in Ti-doped materials.²²

To summarize, we find that $\text{Ca}_3\text{Ru}_2\text{O}_7$, which is a magnetic metal and shows a fascinating array of magnetic and transport properties and phase transitions associated with metal physics, is in fact a strongly Coulomb-correlated material as well in the sense that it is in very close proximity to a Mott transition associated with a G-type AF state. This material, in pristine form and with light Ti doping, provides an excellent system for probing the interplay between correlated metal physics associated with the Fermi surface and Mott physics associated with Coulomb repulsions and orbital physics.

Experimental work at ORNL was supported by the Scientific User Facilities Division, Office of Basic Energy Sciences, DOE; work of D.J.S. was supported by DOE, Materials Sciences and Engineering Division; and the work at Tulane is supported by the DOD ARO under Grant No. W911NF0910530, the NSF under Grant No. DMR-0645305, and the LA-SIGMA program under Award No. EPS-1003897. X.K. gratefully acknowledges the financial support by the Clifford G. Shull Fellowship at ORNL.

*kex1@ornl.gov

¹Y. Kamihara, T. Watanabe, M. Hirano, and H. Hosono, *J. Am. Chem. Soc.* **130**, 3296 (2008).

²I. I. Mazin, D. J. Singh, M. D. Johannes, and M. H. Du, *Phys. Rev. Lett.* **101**, 057003 (2008).

³I. I. Mazin and D. J. Singh, *Phys. Rev. Lett.* **82**, 4324 (1999).

⁴A. P. Mackenzie and Y. Maeno, *Rev. Mod. Phys.* **75**, 657 (2003).

⁵Y. Maeno, H. Hashimoto, K. Yoshida, S. Nishizaki, T. Fujita, J. Bednorz, and F. Lichtenberg, *Nature* **372**, 532 (1994).

⁶R. A. Borzi, S. A. Grigera, J. Farrell, R. S. Perry, S. J. S. Lister, S. L. Lee, D. A. Tennant, Y. Maeno, and A. P. Mackenzie, *Science* **315**, 214 (2007).

⁷F. Baumberger, N. J. C. Ingle, N. Kikugawa, M. A. Hossain, W. Meevasana, R. S. Perry, K. M. Shen, D. H. Lu, A. Damascelli, A. Rost, A. P. Mackenzie, Z. Hussain, and Z. X. Shen, *Phys. Rev. Lett.* **96**, 107601 (2006).

⁸S. Nakatsuji and Y. Maeno, *Phys. Rev. Lett.* **84**, 2666 (2000).

⁹Y. Liu, R. Jin, Z. Q. Mao, K. D. Nelson, M. K. Haas, and R. J. Cava, *Phys. Rev. B* **63**, 174435 (2001).

¹⁰M. Braden, O. Friedt, Y. Sidis, P. Bourges, M. Minakata, and Y. Maeno, *Phys. Rev. Lett.* **88**, 197002 (2002).

¹¹P. Steffens, J. Farrell, S. Price, A. P. Mackenzie, Y. Sidis, K. Schmalzl, and M. Braden, *Phys. Rev. B* **79**, 054422 (2009).

¹²S. V. Halilov, D. J. Singh, J. Minar, A. Y. Perlov, and H. Ebert, *Phys. Rev. B* **63**, 180504(R) (2001).

¹³G. Cao, S. C. McCall, J. E. Crow, and R. P. Guertin, *Phys. Rev. Lett.* **78**, 1751 (1997).

¹⁴Y. Yoshida, I. Nagai, S. I. Ikeda, N. Shirakawa, M. Kosaka, and N. Mori, *Phys. Rev. B* **69**, 220411(R) (2004).

¹⁵J. S. Lee, S. J. Moon, B. J. Yang, J. Yu, U. Schade, Y. Yoshida, S. I. Ikeda, and T. W. Noh, *Phys. Rev. Lett.* **98**, 097403 (2007).

¹⁶Y. Yoshida, S. I. Ikeda, H. Matsuhata, N. Shirakawa, C. H. Lee, and S. Katano, *Phys. Rev. B* **72**, 054412 (2005).

¹⁷W. Bao, Z. Q. Mao, Z. Qu, and J. W. Lynn, *Phys. Rev. Lett.* **100**, 247203 (2008).

¹⁸D. J. Singh and S. Auluck, *Phys. Rev. Lett.* **96**, 097203 (2006).

¹⁹Y. Yoshida, S. I. Ikeda, N. Shirakawa, M. Hedo, and Y. Uwakoto, *J. Phys. Soc. Jpn.* **77**, 093702 (2008).

²⁰D. Fobes, J. Peng, Z. Qu, T. J. Liu, and Z. Q. Mao, *Phys. Rev. B* **84**, 014406 (2011).

²¹S. McCall, G. Cao, and J. E. Crow, *Phys. Rev. B* **67**, 094427 (2003).

²²J. Peng, *et al.*, in preparation (2011).

²³See the Supplemental Material at <http://link.aps.org/supplemental/10.1103/PhysRevB.84.201102>.

²⁴T. Mizokawa, L. H. Tjeng, G. A. Sawatzky, G. Ghiringhelli, O. Tjernberg, N. B. Brookes, H. Fukazawa, S. Nakatsuji, and Y. Maeno, *Phys. Rev. Lett.* **87**, 077202 (2001).

²⁵J. P. Perdew, K. Burke, and M. Ernzerhof, *Phys. Rev. Lett.* **77**, 3865 (1996).

²⁶D. J. Singh and L. Nordstrom, *Planewaves, Pseudopotentials and the LAPW Method*, 2nd ed. (Springer, Berlin, 2006), pp. 1–134.

²⁷E. Sjøstedt, L. Nordstrom, and D. J. Singh, *Solid State Commun.* **114**, 15 (2000).

²⁸P. Blaha, K. Schwarz, G. Madsen, D. Kvasnicka, and J. Luitz, *WIEN2k* (K. Schwarz, Technische Universität Wien, Austria, 2001).

²⁹S. Ray, D. D. Sarma, and R. Vijayaraghavan, *Phys. Rev. B* **73**, 165105 (2006).